A Three-Node Triangular Plate Bending Element Based on Mindlin/Reissner Plate Theory and Mixed Interpolation

Pal-Gap Lee*

(*Received June 13, 1998*)

A new three-node triangular plate bending element, MT3, is presented for linear elastic analysis. MT3 is obtained by separate interpolation of transverse displacements and section rotations, and also of the transverse shear strains. The key to the MITC family element is a proper assumption of strain fields, and in this paper the torsional shear mode present in a standard displacement-based element by one-point reduced integration is exactly incorporated to form the stiffness matrix with two other constant shear modes. The procedure renders the element free of any locking phenomena. Low-order MITC family elements are also compared to the proposed element. A detailed formulation of the plate elemenet is given, and several example solutions are presented that demonstrate the superior predictive capabilities of the element.

Key Words: Mindlin Plate, Shear Locking, Mixed Formulation

1. Introduction

Over the decades considerable effort has been directed toward the development of improved and reliable plate and shell elements, with Mindlin/Reissner theory serving as the canonical starting point in the formulation of conventional 'degenerated' structural elements (see, for a survey, Lee and Sin 1994). There is still great interest in arriving at simple low-order plate/shell elements, especially triangular types which are motivated by their computational cost effectiveness, especially for large-scale nonlinear finite element analysis.

In recent years a group of finite element researchers has concentrated on the development of elements based on Mixed-Interpolated Tensorial Components (i. e. MITC elements), and have proposed: the 4-node MITC4 element (Dvorkin and Bathe, 1984; Bathe and Dvorkin, 1985), the 8-node MITC8 element (Bathe and Dvorkin, 1986) and a complete family of new elements including the triangular MITC7 element (Bathe and Brezzi, 1987; Bathe, Brezzi and Cho, 1989). The MITC family of Mindlin/Reissner elements has a rigorous mathematical foundation that assure the convergence of the discretizations with optimal error bounds for the displacement variables. The theoretical foundations of the elements can be found and additional theoretical and numerical results are presented in several references (see Bathe, Brezzi, 1985; Brezzi and Bathe, 1986; Sussman and Bathe, 1987; Bathe, Brezzi and Cho, 1989). As discussed in the references, the essence of the MITC plate element lies in the separate interpolation of the transverse displacements and section rotations, and also of the transverse shear strains. The displacements and rotations are interpolated as usual, but for the transverse shear strains, the covariant components measured in the natural coordinate system are interpolated. This approach allows the element to be free of locking and insensitive to element distortions. They have proposed additional families of rectangular and triangular elements, which have excellent potential for plate and shell analysis as well.

Up to now, however, lower order MITC plate bending elements, have not been available, especially triangular types; recall that the lowest

* Senior Researcher, Steel Engineering Center, RIST 79-5, Youngcheon, Dongtan Hwasung, 135-777 KoreaK

number of nodes in existing triangular elements is seven (Bathe, Brezzi and Cho, 1989). The main obstacle to designing such a low order triangular element is that the total number of degree of freedom given in the element is too restrictive to properly assume the shear strain field. This fact implies the assumed shear strain has the possibility to contain the property which will still render the element undesirably overstiff.

The objective of this paper is to develop and summarize the formulation of the new MT3 element of the MITC family with only three nodes. The name MITC3 is reserved for the time being to check the property of mostly optimized one. The element is to have a total of nine d. o. f., which corresponds to the lowest order element currently available. The main idea of the element lies in the feature that the shear strain is assumed to have two constant shear strains and a torsional shear mode. The shear strain field is determined by three conditions, which are physical shear strains at the midpoint of each edge of the element. The torsional shear mode corresponds to that obtained by one-point reduced integration in a standard displacement-based element.

In this paper, the plate bending element formulation is first summarized as obtained from the concepts above, and its measured characteristics are then briefly discussed. The discussion also includes the presentation of a number of analysis results on standard benchmark problems found in the literature (Bathe, Brezzi and Cho, 1989; Saleeb, Chang and Yingyeungyong, 1988).

2. The Plate Bending Problem Considered

In this section I summarize the MITC-element policy to circumvent and overcome the locking phenomenon in the plate bending problems to be addressed. Consider first the spaces $\Theta=(H_0^1(\Omega))^2$ and $W=H_0^1(\Omega)$, and a load function f given in $L^2(\Omega)$. The sequence of problems under consideration is:

$$P_t: \inf_{\theta\in\Theta,\, w\in W} \frac{t^3}{2}a(\boldsymbol{\theta},\boldsymbol{\theta})+\frac{\lambda t}{2}\|\boldsymbol{\theta}-\nabla w\|_0^2-t^3(f,w) \quad (1)$$

where $\frac{t^3}{2}a(\boldsymbol{\theta},\boldsymbol{\theta})$ is the bending internal energy, $\frac{\lambda t}{2}\|\boldsymbol{\theta}-\nabla w\|_0^2$ is the shear energy, and $\|\ \ \|_0$ and $(\ ,\ )$ represent respectively the norm and the inner product in $L^2(\Omega)$.

Assume now that we are given the finite element subspaces $\Theta_h\subset\Theta$ and $W_h\subset W$. The corresponding discretized problem is described by

$$\tilde{P}_{th}: \inf_{\theta_h\in\Theta_h,\, w_h\in W_h} \frac{t^3}{2}a(\boldsymbol{\theta}_h,\boldsymbol{\theta}_h) +\frac{\lambda t}{2}\|\boldsymbol{\theta}_h-\nabla w_h\|_0^2-t^3(f,w_h) \quad (2)$$

In general, $\tilde{P}_{th}$ 'locks' for small t. Reducing the influence of the shear energy to a preferred level is a commonly practiced. We consider here the case in which the reduction is carried out in the following way (wich is the essence of the MITC element family): we assume that we are specifically given a third finite element space Γ_h, and a linear operator R which takes values in Γ_h. Then the norm of $\|R(\boldsymbol{\theta}_h-\nabla w_h)\|_0^2$ is taken instead of $\|\boldsymbol{\theta}_h-\nabla w_h\|_0^2$ in the shear energy. It is further assumed that

$$Rw_h=w_h \text{ for all } w_h\subset W_h \quad (3)$$

so that the discretized problem takes the final form

$$P_{th}: \inf_{\theta_h\in\Theta_h,\, w_h\in W_h} \frac{t^3}{2}a(\boldsymbol{\theta}_h,\boldsymbol{\theta}_h) +\frac{\lambda t}{2}\|R(\boldsymbol{\theta}_h-\nabla w_h)\|_0^2-t^3(f,w_h) \quad (4)$$

Setting

$$\boldsymbol{\gamma}=\lambda t^{-2}(\boldsymbol{\theta}-\nabla w) \text{ and } \boldsymbol{\gamma}_h=\lambda t^{-2}(R\boldsymbol{\theta}_h-\nabla w_h) \quad (5)$$

the Euler equations for P_t and P_{th} are

$$a(\boldsymbol{\theta},\boldsymbol{\eta})+(\boldsymbol{\gamma},\boldsymbol{\eta}-\nabla\zeta)=(f,\zeta)\quad \forall\boldsymbol{\eta}\subset\Theta,\ \forall\zeta\subset W \quad (6)$$

and

$$a(\boldsymbol{\theta}_h,\boldsymbol{\eta})+(\boldsymbol{\gamma}_h,R\eta-\nabla\zeta)=(f,\zeta)\quad \forall\boldsymbol{\eta}\subset\Theta_h,\ \forall\zeta\subset W_h \quad (7)$$

respectively. Note here that the operator R is defined mathematically to overcome locking and also to define the 'tying' to be employed between the basis functions used in Γ_h and the functions used in W_h and Θ_h. In Particular, as the thickness of a plate becomes vanishingly small, the limit w obtained will be the solution corresponding to the Kirchhoff model. (see for instance Bathe, Brezzi and Cho, 1989).

3. Details of MT3 Element

The main obstacle to designing a lower-order triangular MITC element is the proper assumption of the shear strain field. As stated in the previous section, the number of degree of freedom in the MT3 element is so restricted that such elements with shear stiffness flexible enough is a difficult procedure. Recalling the fact that the three-node triangular element allows three bending modes including three rigid body motions, either three or four independent shear strain modes are possible. The MT3 element is chosen here to possess three shear strain modes independent of bending modes.

3.1 The finite element discretization

Following the discussion of the previous section, a finite element discretization is characterized by the choice of the finite element spaces and by the choice of the linear operator. Note that these choices are not independent of each other. I introduce below the choice of specific interest in this paper, i. e. the MT3 element, but also briefly summarize the MITC4 and MITC7 element construction (see Fig. 1 and 2). The MITC4 and MITC7 element formulations are only included to indicate the similarity in these element formulations.

For the 3-node triangular MT3 element I use

$$\Theta_h=\{\boldsymbol{\eta}|\boldsymbol{\eta}\subset(H_0^1(\Omega))^2,\ \ \boldsymbol{\eta}|_T\in(P_1)^2\forall\, T\}$$
$$W_h=\{\zeta|\zeta\subset H_0^1(\Omega),\ \ \zeta|_T\in P_1\forall\, T\} \qquad (8)$$

where P_1 is the set of polynomial of degree 1 in each variable corresponding to a standard 3-node element, and T is the current element in the discretization. The space Γ_h is given by

$$\Gamma_h=\{\boldsymbol{\delta}|\boldsymbol{\delta}|_T\in TR(T)\ \ \forall\, T,\ \boldsymbol{\delta}\cdot\boldsymbol{\tau}$$ continu-

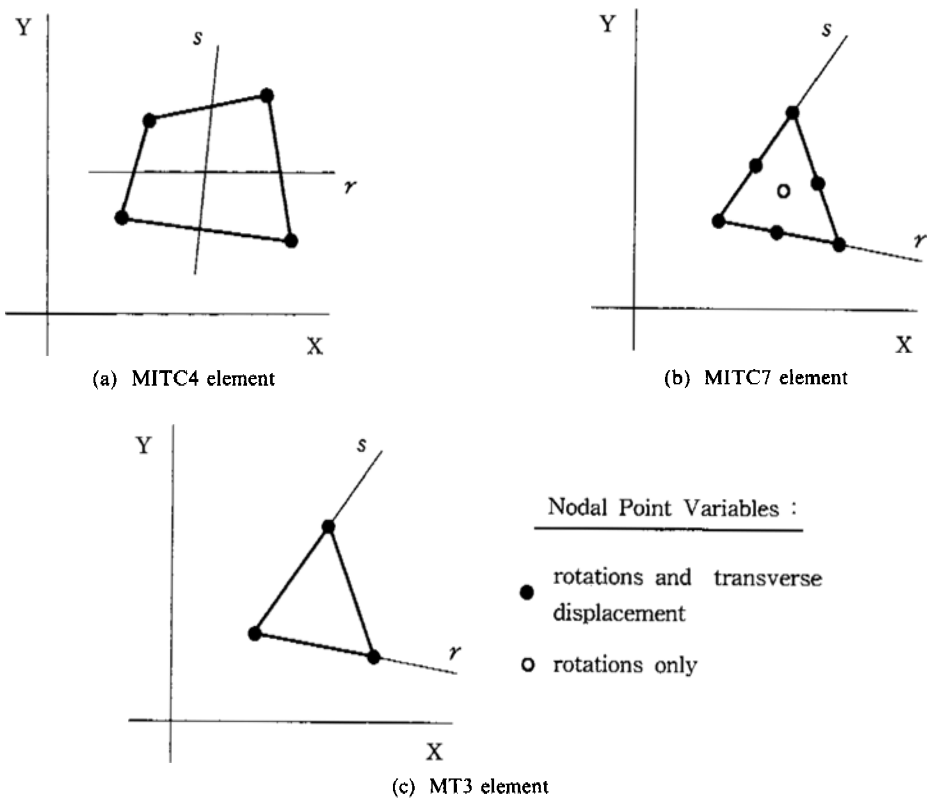

Fig. 1 Plate Bending elements considered.

Table 1 Finite element spaces Θ_h, W_h, Γ_h and linear operator R with tying schemes hired in MTIC-elements

Element	$\Theta_h=\{\eta\|\ldots\}$	$W_h=\{\zeta\|\ldots\}$	$\Gamma_h=\{\delta\|\delta_1=\ldots,\ \delta_2=\ldots\}$		Reduction ope-rator R and Tying scheme
			δ_1	δ_2	
MITC4	$\eta\in(H_0^1(\Omega))^2$ $\eta\|_K\in(Q_1)^2$	$\zeta\in H_0^1(\Omega)$ $\zeta\|_K\in Q_1$	$\delta_1=a_1+b_1y$	$\delta_2=a_2+b_2x$	$\int_e(\eta-R\eta)\cdot\tau ds=0\ \forall\ e$ of K
MITC7	$\eta\in(H_0^1(\Omega))^2$ $\eta\|_T\in(S_7)^2$	$\zeta\in H_0^1(\Omega)$ $\zeta\|_T\in P_2$	$\delta_1=a_1+b_1x+c_1y+y(dx+ey)$	$\delta_2=a_2+b_2x+c_2y-x(dx+ey)$	$\int_e(\eta-R\eta)\cdot\tau p_1(s)\,ds=0$ $\forall\ e$ of T, $\forall\ p_1(s)\in P_1(e)$ $\int_T(\eta-R\eta)\,dxdy=0$
MT3	$\eta\in(H_0^1(\Omega))^2$ $\eta\|_T\in Q_1'$	$\zeta\in H_0^1(\Omega)$ $\zeta\|_T\in Q_1'$	$\delta_1=a_1+by$	$\delta_2=a_2-bx$	$\int_e(\eta-R\eta)\cdot\tau ds=0\ \forall\ e$ of T

ous at the interelement boundaries} (9)

where τ is the tangential unit vector to each edge of the element and

$$TR(T)=\{\delta|\delta_1=a_1+by,\quad \delta_2=a_2-bx\}. \tag{10}$$

we next introduce the reduction operator R by describing its action on the current element: for η smooth in T, $R\eta$ is the unique element in $TR(T)$ that satisfies

$$\int_e(\eta-R\eta)\cdot\tau ds=0,\ \text{for all } e \text{ of } K. \tag{11}$$

Note that if $\eta\in(P_1)^2$ then Eq. (11) is satisfied if and only if $\eta\cdot\tau=R(\eta)\cdot\tau$ at the midpoints of each edge.

In Table 1, the finite element spaces and reduction operator for MITC4 and MITC7 elements are listed for comparison. For the case of MITC4 element, Q_1 is the set of polynomials of degree less than or equal to 1 in each variable for a discretization K. For MITC7 elements, S_7 is a finite dimensional linear space of dimension 7. It can also be characterized as $S_7=P_2\oplus\{\lambda_1\lambda_2\lambda_3\}$, where $\lambda_1\lambda_2\lambda_3$ is the cubic bubble in the discretization T. Using the mean of the values at points TA, TB and TC of the element instead of the integral -tying given in the table, the equation is replaced by [see Fig. 2(a)],

$$\frac{1}{3}(\eta|_{TA}+\eta|_{TB}+\eta|_{TC})=R\eta|_A \tag{12}$$

3.2 Shear strain field

It is broadly known that the stiffness matrix in a conventional three-node triangular element has one spurious zero energy mode when the stiffness matrix is obtained from one-point reduced integration. The three eigenvectors for the shear mode in such a element can be represented as follows:

$$\Psi_t^{\mathrm{T}}=\frac{1}{\sqrt{12}}\begin{array}{c}[0\ 1\ 1\ 0\ -2\ 1\ 0\ 1\ -2]\\ \scriptstyle w_1\ \theta_x^1\ \theta_y^1\ :\ w_2\ \theta_x^2\ \theta_y^2\ :\ w_3\ \theta_x^3\ \theta_y^3\end{array} \tag{13}$$

$$\Psi_x^{\mathrm{T}}=\frac{1}{\sqrt{12}}[0\ 0\ 1\ 0\ 0\ 1\ 0\ 0\ 1] \tag{14}$$

$$\Psi_y^{\mathrm{T}}=\frac{1}{\sqrt{12}}[0\ -1\ 0\ 0\ -1\ 0\ 0\ -1\ 0] \tag{15}$$

where subscript t, x and y in each eigenvectors stand for the torsional mode, constant-xz mode, and constant-yz mode, respectively. The mode in Eq. (13) actually represents the torsional shear strain mode in the natural coordinate plane as depicted in Fig. 3, while the modes in Eq. (14) and (15) are constant shear strain states in each direction. For those eigenvectors three shear strain fields can be calculated, whice are respectively

$$\Gamma_t=\frac{k_t}{\sqrt{12}}\begin{bmatrix}1-3s\\-(1-3r)\end{bmatrix} \tag{16a}$$

$$\Gamma_x=\frac{k_x}{\sqrt{12}}\begin{bmatrix}1\\0\end{bmatrix} \tag{16b}$$

$$\Gamma_y=\frac{k_y}{\sqrt{12}}\begin{bmatrix}0\\1\end{bmatrix} \tag{16c}$$

where k_t, k_x and k_y correspond to the strengths of each mode, respectively. It is to be noted as seen in the equation above that the stiffness matrix obtained from the reduced integration scheme inevitably has a spurious mode, because the shear vanishes at the point of barycenter where one

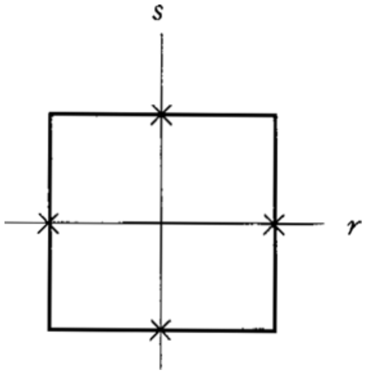

(a) Tying for MITC4 element

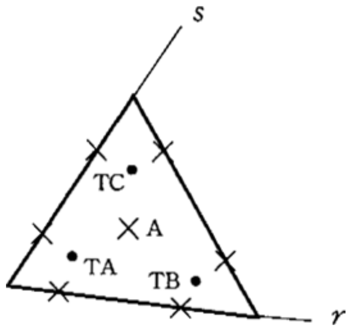

(b) Tying for MITC7 element

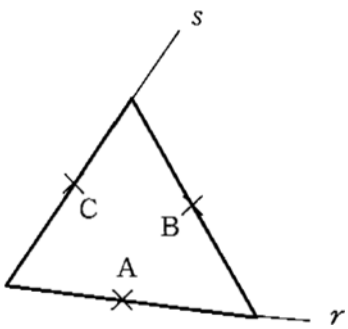

(c) Tying for MT3 element

Fig. 2 Points in each elements used for tying of covariant shear strain components.

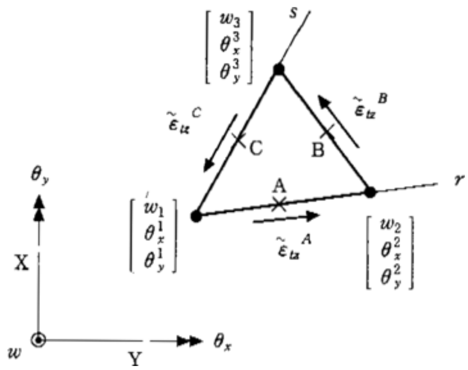

(a) Directions of each sampling strains and nodal variables considered.

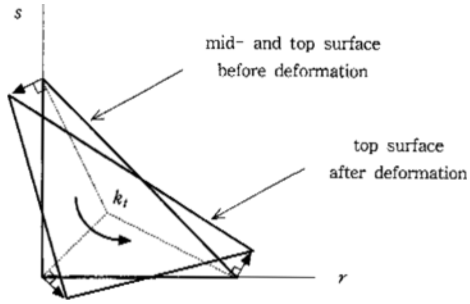

(b) Torsional mode with strength k_t

Fig. 3 Variables in MT3 element and torsional mode.

point integration is carried out in conventional elements.

The total shear strain field is expressed as follows when summed up:

$$\Gamma^{total}=\Gamma_t+\Gamma_x+\Gamma_y=\begin{bmatrix} \dfrac{k_t+k_x}{\sqrt{12}}-\dfrac{3k_t}{\sqrt{12}}s \\ -\dfrac{k_t+k_y}{\sqrt{12}}+\dfrac{3k_t}{\sqrt{12}}r \end{bmatrix} \tag{17}$$

We will use three shear modes above as the basis for the shear strain field in our three node MT3 element.

Consider the element when its geometry is shown in Fig. 3 for which coordinates can be taken as isoparametric coordinates. For this element I use the interpolation

$$\begin{bmatrix} \tilde{\varepsilon}_{rz} \\ \tilde{\varepsilon}_{sz} \end{bmatrix}=\begin{bmatrix} \tilde{\varepsilon}_{tz}{}^{A}-(\tilde{\varepsilon}_{tz}{}^{A}+\sqrt{2}\ \tilde{\varepsilon}_{tz}{}^{B}-\tilde{\varepsilon}_{tz}{}^{C})s \\ -\tilde{\varepsilon}_{tz}{}^{C}+(\tilde{\varepsilon}_{tz}{}^{A}+\sqrt{2}\ \tilde{\varepsilon}_{tz}{}^{B}-\tilde{\varepsilon}_{tz}{}^{C})r \end{bmatrix} \tag{18}$$

where $\tilde{\varepsilon}_{tz}{}^{A}$, $\tilde{\varepsilon}_{tz}{}^{B}$ and $\tilde{\varepsilon}_{tz}{}^{C}$ are shear tensor components at points A, B and C in the directions designated in Fig. 2. Evaluating these strains using the interpolation in Eq. (5), we obtain

$$\tilde{\varepsilon}_{rz}=-w_1-\frac{s}{2}\theta_x^1+\frac{1-s}{2}\theta_y^1+w_2+\frac{s}{2}\theta_x^2 +\frac{1}{2}\theta_y^2+\frac{s}{2}\theta_y^3 \tag{19a}$$

and

$$\tilde{\varepsilon}_{sz} = -w_1 - \frac{1-r}{2}\theta_x^1 + \frac{r}{2}\theta_y^1 - \frac{r}{2}\theta_x^2 + w_3 - \frac{1}{2}\theta_x^2 - \frac{r}{2}\theta_y^3 \quad (19b)$$

With these given interpolations, all strain displacement interpolation matrices can be directly constructed and the stiffness matrix is formulated in the standard manner (Bathe and Dvorkin, 1985).

Considering next the case of a general 3-node element, we use the same basic idea of interpolating the transverse shear strains, but interpolate the covariant tensor components measured as defined in Γ_h as a function of the natural coordinate systems r, s. Hence the strain tensor is given as

$$\boldsymbol{\varepsilon} = \tilde{\varepsilon}_{ij}\, \boldsymbol{g}^i\, \boldsymbol{g}^j \quad (20)$$

where i and j permute over r, s, and t. The covariant base vectors $\boldsymbol{g}^i$ in Eq. (20) are are given calculated from the covariant base vectors $\boldsymbol{g}_i$ (details are given in the Appendix). In this way the element distortion can be directly accounted for.

4. Element Characteristics

The analysis problems studied have been selected to assess the predictive capabilities of the element. Based on the studies up to now, I find the following important element properties (assuming 'full' numerical integration over r and s).

1. The element is able to represent the three rigid body modes. The element contains these modes because zero strains are calculated when the element nodal displacements and rotations correspond to an element rigid body displacement.

2. The element contains no spurious zero energy mode. Spurious zero energy mode which actually occur in a standard 3-node displacement-based triangular element by one-point reduced integration are here exactly calculated by full integration and incorporated into the stiffness matrix of the present element. That means such a mode is a true energy mode in the present element.

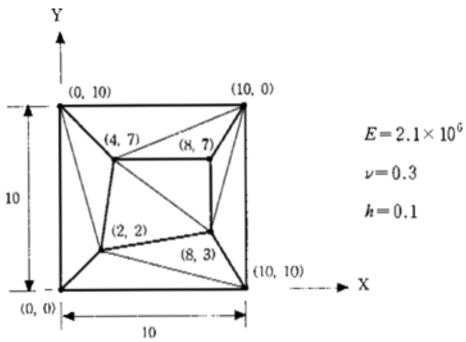

Fig. 4 Patch of elements considered.

3. The element passes the patch test and is applicable to the analysis of very thin plates (i.e., it does not 'lock'). See the numerical solutions in Figs. 8 and 10, and especially Tables 3 and 4.

As regards to the numerical integration it can be found that, even when the element is highly distorted, 3-point standard Gauss integration is adequate.

4.1 Patch test

The patch test has been widely used as a test for element convergence despite its limitations for mixed formulations. I use the test here in numerical form to assess the sensitivity of the element MT3 to geometric distortions. Fig. 4 shows the mesh used for the patch test. The minimum degrees of freedom are constrained to prevent rigid body motions, and for each type of boundary condition and loads the patch tests are passed. Although this simple patch test does not display the complete convergence characteristics of an element, the test does show the sensitivity of an element to geometric distortions, and meets the condition that a reliable element should minimally satisfy (Bathe and Dvorkin, 1986).

4.2 Analysis of a cantilever

I consider here the cantilever described in Fig. 5. In Table 2 I show the results obtained for two types of meshes using the present element. The ratios between finite element and analytical predictions for transverse displacement, rotation and bending moment for extremely thin situation ($L/h=10^5$) are shown to have the same values irrespective of the number of elements used to discretize the cantilever, and also the position of the center node in the 4 element case. It is worth-while to note that the aspect ratios of the finite element used as seen in Fig. 5 are far from that of the master element in Fig. 2, and that finite element solutions are nevertheless very close to the analytical solutions.

Table 2 Analysis of a cantilever. The anaytical solution used as reference is the Bernoulli beam theory solution. Responses of the transverse displacement, rotation and bending moment at tip are normalized with respect to analytical ones respectively, wheras in 4 element case the location of center node is varied ($L/h=10^5$).

Mesh	r	α_1	α_2	α_3
2 elements	-	0.991	0.991	0.991
4 elements	0.125	0.978	0.989	0.989
	0.250	0.989	0.989	0.989
	0.375	0.991	0.991	0.991
	0.500	1.012	1.012	1.012
	0.625	0.987	0.987	0.987
	0.750	1.015	1.015	1.015
	0.875	1.080	1.080	1.080

$\alpha_1=\frac{w^{f.e.m.}}{w^{anal.}}$, $\alpha_2=\frac{\phi^{f.e.m.}}{\phi^{anal.}}$, $\alpha_3=\frac{M^{f.e.m.}}{M^{anal.}}$.

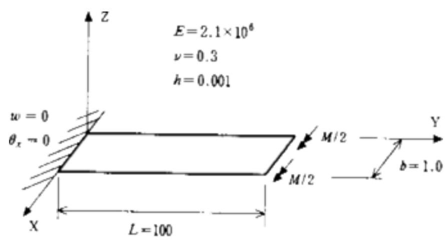

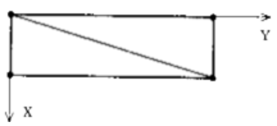

(a) Two element case.

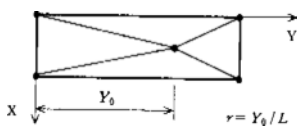

(a) Four element case.

Fig. 5 Cantilever subject to tip bending.

4.3 Analysis of a square plate

Figure 6 shows the plate problems considered and the meshes used in the analysis. Table 3 summarizes the central displacement results obtained for various thicknesses when they are normalized by the analytical Kirchhoff solutions. The meshes of distort-1 and distort-2 in Fig. 7 have been included in the tests in order to identify the distortion sensitivities of the element. It can be observed that the prediction of the low-order element MT3 is remarkable compared to the higher order element MITC7 element. Figure 8 shows the transverse displacement along the centerline of the simply supported plate.

several triangular elements up to now have been proposed to alleviate locking problems, but it is not an easy task to compare directly the predictions of the MT3 element with other C^0 elements as the schemes employed and the interpolation order for calculating the stiffness matrix are quite different. Among the elements, however, we are assured that the HMSH3 element (Saleeb,

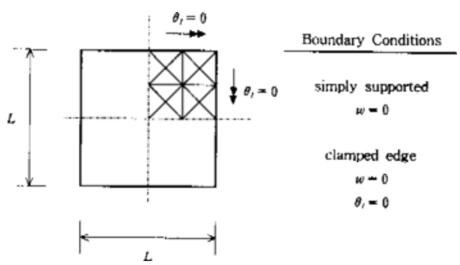

(a) MT3 element mesh layout.

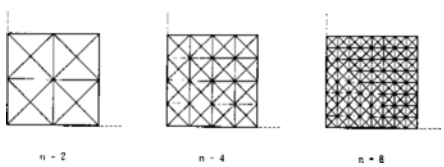

(b) Refinements using MT3 elements.
(n represents no. of elements per side).

Fig. 6 Analysis of a square plate.

Table 3 Analysis of a square plate. The analytical solution used as reference is the Kirchhoff theory solution. (Timoshenko and Woinowsky-Krieger, 1959) (a) Response of MT3 element for various plate thicknesses. (When we attain the value of 1.000, it is Krchhoff's.)

no. of elem./side	thickness	Concentrated load		Uniform pressure	
		simply supported	clamped	simply supported	clamped
2	0.2	0.872	0.703	0.914	0.778
	0.02	0.870	0.698	0.913	0.775
	0.002	0.870	0.698	0.913	0.775
4	0.2	0.961	0.908	0.981	0.943
	0.02	0.958	0.902	0.979	0.939
	0.002	0.958	0.902	0.979	0.939
8	0.2	0.991	0.979	0.999	0.991
	0.02	0.987	0.973	0.996	0.987
	0.002	0.987	0.973	0.996	0.987

(b) Response of the central transverse displacement with respect to analytical solution for distorted mesh layouts under concentrated load at the center of the plate. (thickness=0.02)

Element	Mesh	simply supported	clamped
MT3	distort-1	0.815	0.607
	distort-2	0.934	0.812
MITC4	distort-1	0.986	0.807
	distort-2	0.984	0.922
MITC7	distort-1	0.965	0.827
	distort-2	0.991	0.975

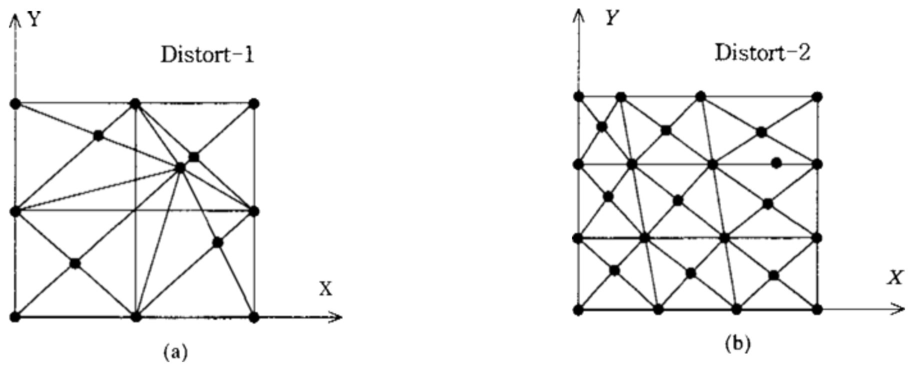

Fig. 7 Distorted mesh layouts for MT3 element. The element distortions are shown to scale.

Chang and Yingyeungyong, 1988) based on hybrid/mixed interpolation using the Hellinger-Reissner principle is one of the most enhanced and outstanding elements, as the element competes favourably with other elements, for instance, DKT(discrete Kirchhoff model element), AST

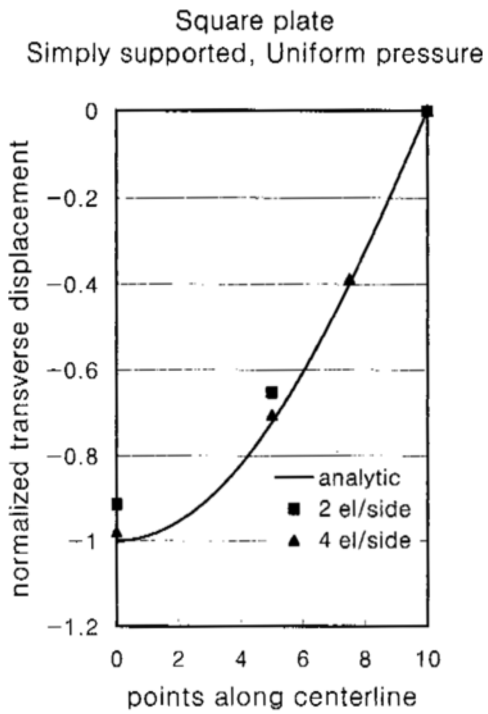

(a) Uniform pressure applied.

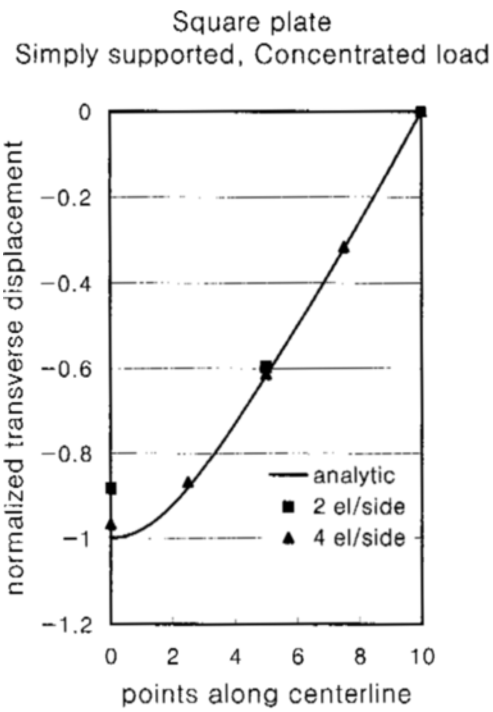

(b) Concentrated load applied at the center of the plate.

Fig. 8 Central displacement response of a simply supported square plate ($L/h=1000$).

(assumed-strain triangular element, Hughes and Taylor), MDT (mode-decomposition, Belytshko et al.) and MIN3 (anisoparametric interpolation, Tessler and Hughes). Comparing the MT3 element with HMSH3 (both triangular type) I found that the results obtained from the analysis of a square plate show the same values even if HMSH3 elements are used in type of macro-element (see the details in Saleeb, Chang and Yingyeungyong, 1988).

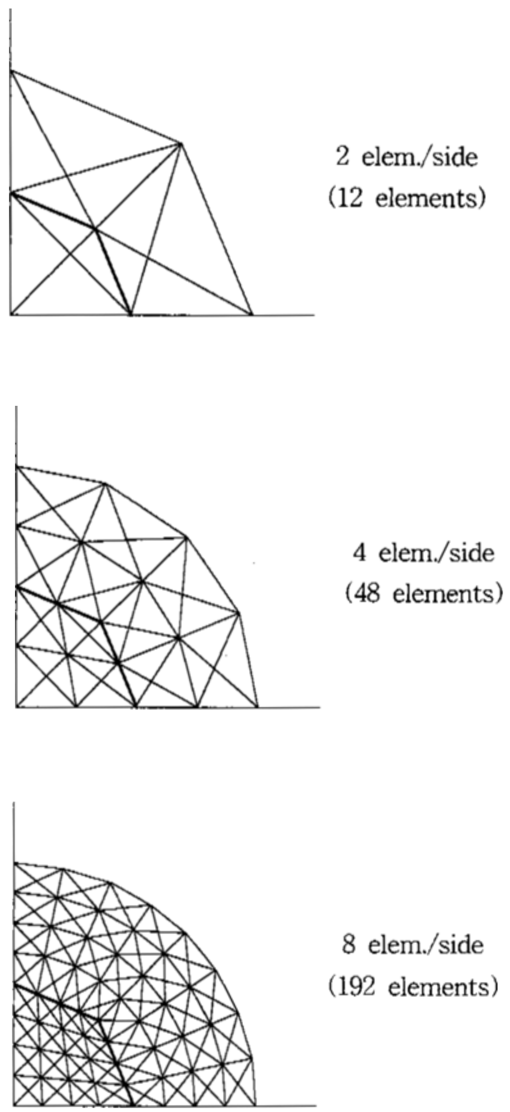

Fig. 9 Finite element meshes for an analysis of a circular plate. Diameter=20, thickness=0.02, $E=2.1\times10^6$ and $\nu=0.3$. Due to symmetry only one quarter of the plate is considered.

With the discussions above note the excellent predictive capabilities of the present element MT3 with no sign of locking i. e., there is little difference in the normalized response as the thickness of the plate becomes vanishingly small.

4.4 Analysis of a circular plate

Figure 9 shows the circular plate problem considered when it is discretized by the meshes used. Table 4 compares the central displacement results with the analytical Kirchhoff solutions. Figure 10 shows the transverse displacement

Table 4 Analysis of a circular plate. The analytical solution used as reference is the Kirchhoff theory solution. (Timoshenko and Woinowsky-Krieger, 1959).

no. of elem./side	thickness	Concentrated load		Uniform pressure	
		simply supported	clamped	simply supported	clamped
2	0.2	0.913	0.600	0.917	0.709
	0.02	0.911	0.593	0.917	0.706
	0.002	0.911	0.593	0.917	0.706
4	0.2	0.971	0.886	0.982	0.926
	0.02	0.968	0.878	0.981	0.924
	0.002	0.968	0.878	0.981	0.924
8	0.2	0.993	0.985	0.996	0.983
	0.02	0.990	0.966	0.995	0.980
	0.002	0.990	0.966	0.995	0.980

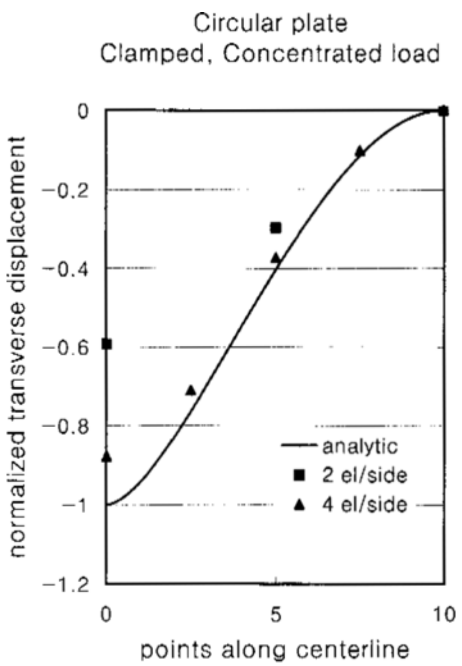

(a) Clamped edge.

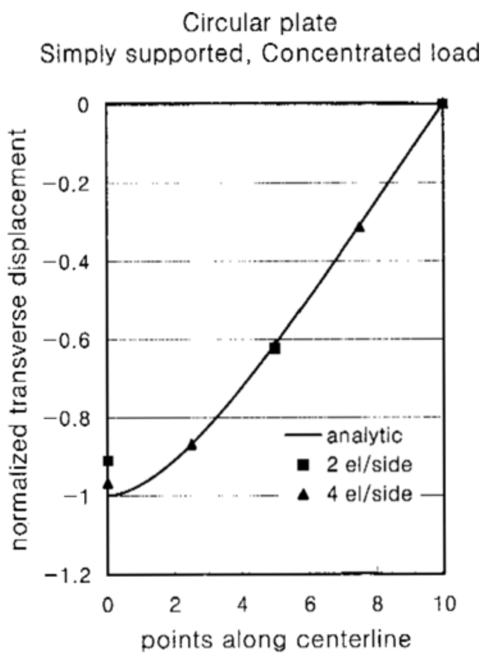

(a) Simply supported edge.

Fig. 10 Central displacement response of a circular plate with concentrated load at the center ($R/h=1000$).

along the centerline of the simply supported and the clamped circular plate with uniform pressure loading condition. When compared with the HMSH3 element, approximately the same level of solution accuracy is obtained even though the two elements are formulated through totally different approaches (Saleeb, Chang and Yingyeungyong, 1988). As in the analysis of the square plate, there is little difference between the results obtained when the thickness is either moderately thick or very thin.

5. Conclusions

The objective in this paper has been to present in a compact manner a three- node plate bending element that is obtained from the proper assumption of shear strain field, in which the three independent shear modes can be described. Among the modes, the torsional shear mode, which inevitably leads to the spurious zero energy mode if we employ one-point integration in a 3-node standard displacement-based element, is evaluated exactly to form the stiffness matrix. Various example problems are tested using the present element, and the results show that it is free of shear locking and applicable to both thin and thick plates with excellent predicitive capabilities. The concepts employed here may be extended to higher-order triangular elements with less than 7 nodes. Present research in this direction suggests that the restricted number of d. o. f., for instance, the triangular MITC4 element containing one bubble node at the barycenter, renders the design of this new element implausible, as the stiffness matrix is still overestimated. I believe a proper assumption of the shear strain field needs more time to fulfill that requirements the sound robust elements should necessarily possess.

References

Lee, P. -G. and Sin, H.-C., 1994, "Mindlin Plate Finite Elements by a Modified Transverse Displacement," *KSME International Journal*, Vol. 8, No. 1, pp. 19~27.

Bathe, K. J. and Brezzi, F., 1985, "On the Convergence of a Four-Node Plate Bending Element Based on Mindlin-Reissner Plate Theory and a Mixed Interpolation," *Conference on Mathematics of Finite elements and Applications* V (Edited by Whiteman, J. R.), Academic Press, New York, pp. 491~503.

Bathe, K. J. and Brezzi, F., 1987, "A Simplified Analysis of Two Plate Bending Elements the MITC4 and MITC9 Elements," *Proc. NUMETA Conf*., University College of Swansea, Wales.

Bathe, K. J., Brezzi, F. and Cho, S. W., 1989, "The MITC7 and MITC9 Plate Bending Elements," *Comput. Struct*. Vol. 32, pp. 797~814.

Bathe, K. J. and Dvorkin, E., 1985, "A Four -Node Plate Bending Element Based on Mindlin -Reissner Plate Theory and a Mixed Interpolation," *Int. J. Numer. Meth. Engng*., Vol. 21, pp. 367~383.

Bathe, K. J. and Dvorkin, E. 1986, "A Formulation of General Shell Elements: The Use of Mixed Interpolation of Tensorial Components," *Int. J. Numer. Meth. Engng*., Vol. 22, pp. 697 ~722.

Brezzi, F. and Bathe, K. J., 1986, "Studies of Finite Element Procedures the Inf-Sup Condition, Equivalent Forms and Applications," *Conference on Reliability of Methods for Engineering Analysis* (Edited by Bathe, K. J. and Owen, D. R. J.), Pineridge Press, Swansea.

Dvorkin, E. and Bathe, K. J., 1984, "A Continuum Mechanics Based Four-Node Shell Element for General Nonlinear Analysis," *Engng Comput*., Vol. 1, pp. 77~88.

Green, A. E. and Zerna, W., 1968, *Theoretical Elasticity*, 2nd edn, Oxford University Press.

Raviart, P. A. and Thomas, J. M., 1975, "A Mixed Finite Element Method for Second-Order Elliptic Problems," *In Mathematical Aspects of Finite Element Methods*, Lecture Notes in Mathematics, Vol. 606, Springer, Berlin, pp. 292~315.

Saleeb, A. F., Chang, T. Y. and Yingyeunyong, S., 1988, "A Mixed Formulation of C^0-Linear Triangular Plate/Shell Element the Role of Edge Shear Constraints," *Int. J. Numer. Meth. Engng*., Vol. 26, pp. 1101~1128.

Sussman, T. and Bathe, K. J., 1987, "A Finite Element Formulation for Nonlinear Incompressible Elastic and Inelastic Analysis," *Comput. Struct.*, Vol. 26, pp. 357~409.

Timoshenko, S. P. and Woinowsky-Krieger, S., 1959, *Theory of Plates and Shells*, 2nd Edn. McGraw-Hill.

Appendix:

Derivation of Transverse Shear Interpolations

In the natural coordinate system of the plate bending element, the covariant vectors are defined as (Green and Zerna, 1968),

$$g_r=\frac{\partial x}{\partial r}\ ;\ g_s=\frac{\partial x}{\partial s}\ ;\ g_t=\frac{h}{2}e_3 \qquad (A.\ 1)$$

where x is the vector of coordinates, $x=xe_1+ye_2$ and the e_i are the base vectors of the Cartesian system.

The contravariant base vectors g^i are defined by the following expression:

$$g^i\cdot g_j=\delta^i_j \qquad (A.\ 2)$$

where the are δ^i_j mixed components of the Kronecker delta, and i, j vary over r, s, t.

The following relation also holds:

$$g_{ij}=g_i\cdot g_j$$
$$g^i=g^{ij}g_j$$
$$g^{ij}=\frac{4D_{ij}}{h^2(\det J)^2} \qquad (A.\ 3)$$

where D^{ij} is cofactor of the term g_{ij} in the 3×3 matrix of the metric tensor,

In the natural coordinate system, the strain tensor can be expressed using covariant tensor components and the contravariant base vectors,

$$\varepsilon=\tilde{\varepsilon}_{ij}\ g^i\ g^j \qquad (A.\ 4)$$

where the tilde indicates that the tensor components are measured in the natural coordinate system.

To obtain the shear strain tensor components we now use the followings,

$$\begin{bmatrix}\tilde{\varepsilon}_{rz}\\ \tilde{\varepsilon}_{sz}\end{bmatrix}=\begin{bmatrix}\tilde{\varepsilon}_{tz}{}^A-(\tilde{\varepsilon}_{tz}{}^A+\sqrt{2}\ \tilde{\varepsilon}_{tz}{}^B-\tilde{\varepsilon}_{tz}{}^C)s\\ -\tilde{\varepsilon}_{tz}{}^C+(\tilde{\varepsilon}_{tz}{}^A+\sqrt{2}\ \tilde{\varepsilon}_{tz}{}^B-\tilde{\varepsilon}_{tz}{}^C)r\end{bmatrix} \qquad (A.\ 5)$$

where $\tilde{\varepsilon}_{tz}{}^A$, $\tilde{\varepsilon}_{tz}{}^B$ and $\tilde{\varepsilon}_{tz}{}^C$ are shear tensor components at points A, B and C. These quantities are evaluated using the linear terms of the relation (Green and Zerna, 1968),

$$\tilde{\varepsilon}_{ij}=\frac{1}{2}[{}^1g_i\cdot{}^1g_j-{}^0g_i\cdot{}^0g_j] \qquad (A.\ 6)$$

where the left superscript of the base vectors is equal to '1' for the deformed configuration and equal to '0' for the initial configuration.

Then the shear strain values at each sampling point are

$$\tilde{\varepsilon}_{tz}{}^A=\frac{h}{4}\Big[\frac{A_{21}}{2}(\theta_y^1+\theta_y^2)-\frac{B_{21}}{2}(\theta_x^1+\theta_x^2)+(-w_1+w_2)\Big] \qquad (A.\ 7a)$$

$$\sqrt{2}\,\tilde{\varepsilon}_{tz}{}^B=\frac{h}{4}\Big[\frac{A_{32}}{2}(\theta_y^2+\theta_y^3)-\frac{B_{32}}{2}(\theta_x^2+\theta_x^3)+(-w_2+w_3)\Big] \qquad (A.\ 7b)$$

and

$$-\tilde{\varepsilon}_{tz}{}^C=\frac{h}{4}\Big[-\frac{A_{13}}{2}(\theta_y^1+\theta_y^3)+\frac{B_{13}}{2}(\theta_x^1+\theta_x^3)+(-w_1+w_3)\Big] \qquad (A.\ 7c)$$

Next in order to make the element insensitive to element distortion we use that

$$\tilde{\varepsilon}_{ij}\ g^i\ g^j=\varepsilon_{kl}e_ke_l \qquad (A.\ 8)$$

where the ε_{kl} are the components of the strain tensor measured in the Cartesian coordinate system.

From Eq. (A. 8) we obtain

$$\gamma_{xz}=2\tilde{\varepsilon}_{rt}(g^r\cdot e_x)(g^t\cdot e_t)+2\tilde{\varepsilon}_{st}(g^s\cdot e_x)(g^t\cdot e_t) \qquad (A.\ 9a)$$

$$\gamma_{yz}=2\tilde{\varepsilon}_{rt}(g^r\cdot e_y)(g^t\cdot e_t)+2\tilde{\varepsilon}_{st}(g^s\cdot e_y)(g^t\cdot e_t) \qquad (A.\ 9b)$$

but

$$g^r=\sqrt{g^{rr}}(\sin\beta e_x-\cos\beta e_y) \qquad (A.\ 10a)$$
$$g^s=\sqrt{g^{ss}}(-\sin\gamma e_x+\cos\gamma e_y) \qquad (A.\ 10b)$$
$$g^t=\sqrt{g^{tt}}\,e_t \qquad (A.\ 10c)$$

where α and β are the angles between the x- and r-axis, and x- and s-axis, respectively.

Also Eq. (A. 3) are

$$g^{rr}=\frac{A_{13}{}^2+B_{13}{}^2}{(\det J)^2} \qquad (A.\ 11a)$$

$$g^{ss}=\frac{A_{21}{}^2+B_{21}{}^2}{(\det J)^2} \qquad (A.\ 11b)$$

$$g^{tt}=\frac{4}{h^2} \qquad (A.\ 11c)$$

where the A_{21}, B_{21}, A_{32}, B_{32}, A_{13} and B_{13} are defined in (A. 16).

With these interpolations given, all strain displacement interpolation matrices can be directly constructed and the stiffness matrix is formulated in the standard manner.

$$\gamma_{xz}=\gamma_{rz}\sin\beta-\gamma_{sz}\sin\alpha \tag{A. 12a}$$

$$\gamma_{yz}=\gamma_{rz}\cos\beta-\gamma_{sz}\cos\alpha \tag{A. 12b}$$

where α and β are the angles between the r- and x-, and s- and x- axis, respectively, and also

$$\gamma_{rz}=\frac{\sqrt{A_{13}{}^2+B_{13}{}^2}}{\det J}$$

$$\Big[-w_1-\frac{B_{21}+B_{32}s}{2}\theta_x^1+\frac{A_{21}+A_{32}s}{2}\theta_y^1$$

$$+w_2-\frac{B_{21}+B_{13}s}{2}\theta_x^2+\frac{A_{21}+A_{13}s}{2}\theta_y^2$$

$$-\frac{B_{21}s}{2}\theta_x^3+\frac{A_{21}s}{2}\theta_y^3\Big] \tag{A. 13}$$

$$\gamma_{sz}=\frac{\sqrt{A_{21}{}^2+B_{21}{}^2}}{\det J}$$

$$\Big[-w_1+\frac{B_{13}+B_{32}r}{2}\theta_x^1-\frac{A_{13}+A_{32}r}{2}\theta_y^1$$

$$+\frac{B_{13}r}{2}\theta_x^2-\frac{A_{13}r}{2}\theta_y^2$$

$$+w_3+\frac{B_{13}+B_{21}r}{2}\theta_x^3-\frac{A_{13}+A_{21}r}{2}\theta_y^3\Big] \tag{A. 14}$$

In Eq. (A. 11), (A. 13) and (A. 14)

$$\det J=\det\begin{bmatrix}\frac{\partial x}{\partial r} & \frac{\partial y}{\partial r}\\ \frac{\partial x}{\partial s} & \frac{\partial y}{\partial s}\end{bmatrix} \tag{A. 15}$$

and

$$A_{21}=x_2-x_1\ ;\ A_{32}=x_3-x_2\ ;\ A_{13}=x_1-x_3$$
$$B_{21}=y_2-y_1\ ;\ B_{32}=y_3-y_2\ ;\ B_{13}=y_1-y_3 \tag{A. 16}$$